Differential anharmonicity and thermal expansion coefficient in 3*C*-SiC nanowires

Zubaer M. Hossain,* Fazle Elahi, and Zhaocheng Zhang
Laboratory of Mechanics & Physics of Heterogeneous Materials, Department of Mechanical Engineering, University of Delaware, Newark, Delaware 19716, USA

(Received 5 November 2018; revised manuscript received 17 January 2019; published 8 March 2019)

Surface and core are two essential but distinct structural parts of a nanowire—but their individual effects on overall thermal expansion coefficient of a nanowire have never been quantified. Here we present an average bond-length based framework to determine the effects of the surface and core regimes of 3*C*-SiC nanowires on their effective volumetric thermal expansion coefficient over a wide range of temperatures. Our results suggest that the surface and core atoms exhibit differential anharmonic response at finite temperatures, which makes the surface regime exhibit disparate expansion behavior compared to the core. While at lower temperatures the differential anharmonicity is negligible, at temperatures higher than the room temperature there is a pronounced differential anharmonicity in the nanowire. Furthermore, temperature-dependent expansion coefficients of the nanowire and the surface and core regimes qualitatively follow the behavior of the bulk—but they vary substantially quantitatively, with the maximum coefficient exhibited by the surface at higher temperatures. The diameter-dependent expansion coefficients follow inverse power laws with their exponents varying from 0.95 to 2.5. In thinner nanowires the expansion coefficient is controlled by an intricate combination of mass inertia and bond stiffness at the surface and core, whereas the expansion of thicker nanowires is dominated by the anharmonic motion of the core atoms alone. The surface effects saturate with increasing diameter, but the core effects decay nonlinearly with increasing diameter and approaches the bulk value as $d \to \infty$.

DOI: 10.1103/PhysRevB.99.115407

I. INTRODUCTION

Low-dimensional materials such as nanowires, nanotubes, and nanoparticles have many critical applications in a variety of fields including electronics, thermoelectrics, composites, biomedicine, and nanoelectronics. Size has been shown to play a significant role in altering thermal conductivity in brittle nanowires [1–6] and melting temperature of metallic nanoparticles [7,8]. Nonetheless it remains less understood how diameter of a nanowire affects its thermal expansion coefficient (TEC), and more importantly how the surface versus core regimes govern the overall thermal expansion behavior of a nanowire remains unexplored. The main difficulty arises from (i) defining the surface versus core regimes that are relevant to thermal expansion and (ii) inadequacies in theoretical frameworks that can capture the effects of nanostructural features on thermal expansion in low-dimensional materials. In this paper, we propose a bond-length-based approach to calculate volumetric TEC in nanowires and use the approach to determine the relative contributions of surface versus core on effective volumetric TEC of nanowires.

Thermal expansion plays a crucial role in regulating formation of defects and stress in multimaterial systems under operating conditions involving finite temperatures. Also the coefficient of thermal expansion is a critical property of a material that governs a variety of thermomechanical state of a solid including thermal stress, thermal shock, surface cracking or crack nucleation, and thermal failure [9]. While the physics of thermal expansion is well-known for many materials in their bulk configuration [10–17], analogous information remains limited to a few nanostructured solids [18–23]. More importantly, the effects of different characteristic structural features (such as surface, core, and diameter) and their correlative influence on macroscopic expansion behavior have never been quantified. Consequently there is a knowledge gap in understanding if and how a surface behaves differently compared to the core so that their differential response can be exploited in sensing applications or in controlling the expansion of a nanowire by engineering its surface. Moreover, a correct measure of their contributions can enable engineering the effective thermal expansion in nanowire-reinforced composites wherein surface atoms govern the mechanical compatibility and coherence of a nanowire with a second material.

With an objective of determining the effect of surface and core atoms on effective thermal expansion coefficient of nanowires, we consider 3*C*-SiC as an example material due to its high impact in a variety of applications [24–32]. The exceptional properties of SiC arise from high resistance to thermal damage [33], large mechanical stability and strength at high-temperatures [34], higher chemical inertness [35], and outstanding insulating properties [36]. Similar to bulk SiC, nanowire SiC has also drawn wide attention in a number of applications areas including aerogel [37], thermoelectrics [38], thermal barrier coatings [39], biomaterials [40], electronics [41], photochemistry [42], photoluminescence [43], and hydrogen storage [44]. These versatile applications and promise in new emerging applications [45,46] motivate an in-depth understanding of their atomic scale expansion mechanisms for attaining improved, tailorable,

*zubaer@udel.edu

and functional performance from nanowires in advanced applications.

To calculate thermal expansion of a nanowire, the linear thermal expansion coefficient (LTEC) is usually used, with a number of simplifying assumptions in accounting for the variations in diameter and associated heterogeneity in bond deformation [47,48]. There is a general understanding that presence of surface and associated mechanical phenomena influences the thermomechanical properties of nanowires. Existing explanations of thermal expansion coefficients are developed primarily based on surface stress or eigenstrain. Nonetheless, recent findings contradict surface-stress-based explanations and show other factors such as nonlinear elasticity at the core [49] and energy density at the surface [50] to affect the mechanical state of a nanowire with a potential influence on thermal expansion. To maintain the condition of zero pressure, the macroscopic mechanical condition for a solid under thermal expansion remains stress free, regardless of the temperature of the system. The expansion of a solid under temperature gradient but no mechanical constraint is strictly controlled by the thermal gradient and associated anharmonic response of the solid, prescribed by the coefficient of volumetric thermal expansion. This therefore rules out the possibility of surface stress as the key ingredient for controlling thermal expansion in nanowires. Here we show that variation in potential energy density affecting the softening and stiffening state of the bonds plays the most important role in governing thermal expansion of brittle nanowires.

Unlike the linear thermal expansion coefficient (denoted here as α), the volumetric thermal expansion coefficient (VTEC) requires the complete knowledge of the dimensional change in all directions in a vector space—unless the solid is isotropic possessing cubic symmetry and pertaining to the uniform strain state so that strain invariance is applicable regardless of the thermal state of the system. By definition the mathematical form of volumetric thermal expansion coefficient is written as [51]

$$\beta = \frac{1}{V_T}\frac{\partial V_T}{\partial T}\bigg|_p = \frac{d\ln V_T}{dT}\bigg|_p, \tag{1}$$

where V_T is volume at temperature T and the temperature derivative is evaluated at constant pressure P.

For a bulk solid, Eq. (1) is a well-defined relation to apply, as volume V_T is easily calculable from the equilibrium macroscopic dimension. However, for nanowires, the difficulty in capturing their radial dimension at finite temperatures makes it a nontrivial task to compute diameter or macroscopic volume [52] and, therefore, β. For example, determination of the diameter of a nanowire from the macroscopic projection of the atomic coordinates (on the plane perpendicular to the axial direction) invokes inaccuracies arising from thermal fluctuations of the nanowire as well as the random movements of the surface atoms [47,48]. The situation becomes more intricate at higher temperatures. Although an estimation of α for the nanowire can be extracted from the box dimension along the axial direction, it does not provide information on the individual roles of the surface and core atoms. Furthermore identifying the surface and core regimes of a nanowire at finite temperatures becomes another nontrivial issue to address. As a result the relative contributions of surface and core atoms are mostly unfeasible from macroscopic understanding of thermal expansion. To address the difficulty, we propose to calculate β directly from a bond-length-based approach that eliminates the need for calculating diameter but yet enables predicting VTEC for the core and surface atoms as well as the nanowire. We applied the approach to investigate VTEC of [111] 3*C*-SiC nanowires for 1.0–6.35 nm diameters at 1 to 1500 K. We find the nanowires to show higher thermal expansion coefficient compared to the bulk—and the surface atoms contribute to thermal expansion differently than the core atoms. The underlying mechanisms are governed by diameter-dependent potential energy density and differential anharmonicity in atomic motion between the bulk and surface atoms.

The paper is organized as follows. In Sec. II, we describe and discuss the theoretical approach introduced to study β; in Sec. III, we validate that approach for bulk SiC and investigate the role of core and surface atoms on overall macroscopic thermal expansion behavior of the nanowires.

II. THEORETICAL APPROACH

Thermal expansion of a solid arises from the asymmetry in vibrational energy versus atomic separation, and the coefficient of thermal expansion is a measure of vibrational amplitude difference due to increase in temperature. Based on the quasiharmonic approximation [53,54], the linear expansion coefficient is calculated from the phonon band structures as [55–57]

$$\alpha(T) = \frac{1}{3B_0}\sum \gamma_n(\vec{q})C_n(\vec{q}), \tag{2}$$

where B_0 is the bulk modulus, $\gamma = -d\ln\omega_n(\vec{q})/d(\ln V)$ is the mode-dependent Gruneisen parameter, $C_n(\vec{q})$ the mode-dependent specific heat, and the sum runs over the phonon modes n with wave vector $\vec{q}$. The mode-dependent $C_n(\vec{q})$ is defined as

$$C_n(\vec{q}) = \frac{\hbar^2\omega_n^2(\vec{q})}{Vk_bT^2}\frac{\exp\frac{\hbar\omega_n(\vec{q})}{k_bT}}{\left(\exp\frac{\hbar\omega_n(\vec{q})}{k_bT}-1\right)^2}. \tag{3}$$

The above relation can be simplified to

$$C_n(\vec{q}) = \frac{1}{2Vk_b}\left(\sum_{i=2,4,6}\frac{\hbar^{i-2}\omega_n^{i-2}(\vec{q})}{i!k_b^iT^{i-2}}\right)^{-1} \tag{4}$$

by expanding the sum up to the sixth order in T (and considering that the terms with orders equal to or higher than the eight order have negligible effect, particularly at higher temperatures). In this model, temperature dependence of α appears through C_n; and its effect on α is inversely proportional to the inverse of a sum of T^{i-2} terms, and their combined effects approach a constant value at higher temperatures. Thus, for most materials, the asymptotic trend of α at higher T is governed primarily by the derivative of the Bose-Einstein factor.

Application of Eq. (4) for nanowires is however a difficult task, because of the large computational cost required for phonon calculations from first-principles calculations as well as in determining γ_n at different volumes of the nanowires.

Furthermore, identifying the contributions of the core atoms and surface atoms on the expansion coefficient of a nanowire involves a tedious task of decomposing the corresponding phonon modes and deriving their influence on the Gruneisen parameter and specific heat. As an alternative, classical molecular dynamics simulations can be performed. It has been successfully applied to obtain reliable thermal properties of semiconductors [1–4] as well as to determine the linear thermal expansion coefficient α for a number of cubic solids including Si [51], SiC [58], and C [59,60] for their bulk configuration, where α is obtained from the macroscopic change in length or $\partial \ln l/\partial T$. It is straightforward to calculate dimensional change of a bulk and α. However, it is a difficult to compute β of a NW from its macroscopic geometric information particularly at higher temperatures, due to random fluctuations of the atoms at the surface and the difficulty in capturing diameter.

To address the difficulties, we propose to exploit the relationship between macroscopic volume and bond length: $V = NA\bar{r}^3$, where V is the macroscopic volume, N is the number of atoms in the system, A is a proportionality parameter (which depends on the crystal structure of a lattice), and $\bar{r}$ is the ensemble average bond length. At equilibrium, an analytical estimate of A can be obtained from the structural parameters of the unit cell. The volume of the unit cell with lattice constant a containing eight atoms is $V_{\text{macro}} = a^3 = (4\bar{r}/\sqrt{3})^3$, where V_{macro} denotes the volume of the unit cell obtained from the macroscopic or cell dimension. If we are to calculate the same volume from the average bond length $\bar{r}$, we can write $V_{\text{atomistic}} = NA\bar{r}^3 = 8A\bar{r}^3$, where $V_{\text{atomistic}}$ is the volume of the same unit cell obtained from the atomistic information or bond length, and the constant $N = 8$ is the number of atoms in the unit cell. Since both V_{macro} and $V_{\text{atomistic}}$ refer to the same volume of the unit cell, we set $V_{\text{macro}} = V_{\text{atomistic}}$ and obtain $A = 1.5396$. It should be noted here that in the definition of $V_{\text{atomistic}}$, an effective atomic volume is assigned to each atom by the quantity $A\bar{r}^3$, where the quantity A is related to the shape of the effective atomic volume.

The general expression for the volumetric expansion coefficient can thus be written for a bulk as

$$\beta_{\text{bulk}} = \frac{d \ln V_{\text{macro}}}{dT} = \frac{d \ln V_{\text{atomistic}}}{dT} = 3\frac{d \ln \bar{r}}{dT}. \tag{5}$$

Here, the term $\frac{d \ln \bar{r}}{dT}$ refers to the linear thermal expansion coefficient or α, proving that the volumetric expansion coefficient is three times the linear expansion coefficient (as often used in relating linear expansion with volumetric expansion for cubic solids). In Eq. (5), the relation $\frac{d \ln V_{\text{atomistic}}}{dT} = 3\frac{d \ln \bar{r}}{dT}$ implies that $NA\bar{r}^3 = A\sum \bar{r}_i^3$, where $\bar{r}$ is the average bond length in the ensemble and $\bar{r}_i$ is the average length of the bonds connected to the atom at site i. For bulk configurations, $\bar{r} = \bar{r}_i$, whereas for nanostructures, $\bar{r}$ may not be equal to $\bar{r}_i$ due to the presence of the surface. As we show later, there is no significant spatial variation in bond lengths in the core or the surface regimes in SiC nanowire over a large temperature range. It is thus reasonable to approximate $\bar{r} = \bar{r}_i$. As the temperatures of the system increases, bond lengths form a Maxwell-Boltzmann type distribution due to thermal fluctuations. At a given temperature, some bonds are longer than the ensemble averaged bond length and some are smaller. The higher the temperature the wider is the range of bond length. Yet $\bar{r} = \bar{r}_i$ holds in each of the surface and core regimes that can be reasonably justified from an analytical analysis as described below.

Let us denote the change in bond length relative to the ensemble averaged bond length as Δr. Using Taylor's expansion we can then write, $(\bar{r} \pm \Delta r)^3 = \bar{r}^3 \pm 3(\Delta r)\bar{r}^2 + 3(\Delta r)^2\bar{r} \pm \mathcal{O}(\Delta r)^3 = \bar{r}^3 + 3(\Delta r)^2\bar{r} + \mathcal{O}(\Delta r)^4$. Since thermal expansion coefficient is a first order effect and $(\Delta r)^2 \ll \Delta r$, we can conclude that $(\bar{r} \pm \Delta r)^3 = \bar{r}^3$ is a reasonable approximation for computing the thermal expansion coefficient. In situations where large spatial variations in bond lengths are possible, consideration of $A\sum \bar{r}_i^3$ (instead of $NA\bar{r}$) may result in a more accurate estimation of $V_{\text{atomistic}}$. To test this for the current work, we used $NA\bar{r}^3$ and $A\sum \bar{r}_i^3$ to expression the volumes of the core and surface and obtain identical results, suggesting the condition that $\bar{r} = \bar{r}_i$ is a reasonable approximation in each of the surface and core regimes. The use of $NA\bar{r}^3$ in describing volume simplifies the expression for β and makes it calculable directly from the ensemble averaged statistical quantities. It should however be pointed out that average bond length based description of thermal expansion coefficient does not take into account anisotropic effects of macroscopic thermal motion arising from difference in boundary conditions in the nanowire.

The ensemble averaged bond-length based description offers an atomistic platform for uncovering the physics of thermal expansion in terms of local variations in atomic scale features (such as surfaces, defects, impurity, etc.). Also, it allows determination of β directly from its local atomistic ingredients as we show next. We demonstrate its usefulness in enabling an accurate quantification of the relative contributions of the surface versus bulk atoms on overall β of a nanowire. In this approach, the volume of the nanowire is decomposed into the volumes of core and surface as follows:

$$V_{\text{nw}} = V_{\text{core}} + V_{\text{surface}} \tag{6}$$

$$= AN_c\bar{r}_c^3\left(1 + \frac{N_s}{N_c}\frac{\bar{r}_s^3}{\bar{r}_c^3}\right), \tag{7}$$

where N_s and N_c are the number of bonds of the surface and core atoms, respectively; $\bar{r}_s$ and $\bar{r}_c$ are the average bond length in the surface and core regimes, respectively; and A is assumed to be the same for the surface and the core and temperature independent. It should be noted that structural variation (such as surface reconstruction) can result in different values of A for the surface and the core. In this work, no surface reconstruction was observed for the nanowires. Furthermore, we estimate negligible dependence of A on temperature so that it is reasonable to set $\frac{dA}{dT} = 0$. The expressions for β_{core}, β_{surface}, and β_{nw} are therefore

$$\beta_{\text{core}} = 3\frac{d \ln \bar{r}_c}{dT}, \tag{8}$$

$$\beta_{\text{surface}} = 3\frac{d \ln \bar{r}_s}{dT}, \text{ and} \tag{9}$$

$$\beta_{\text{nw}} = \beta_{\text{c}} + \frac{d \ln\left[1 + \frac{N_s}{N_c}\left(\frac{\bar{r}_s}{\bar{r}_c}\right)^3\right]}{dT}. \tag{10}$$

It is clear from the equations that the thermal expansion coefficient is not an additive quantity, so that

$$\beta_{\rm nw} \neq \beta_{\rm surface} + \beta_{\rm core}. \tag{11}$$

Furthermore, to describe the difference in the anharmonic response of the surface and core atoms we define a quantity called "differential anharmonicity" as the difference in the average bond length in the surface and core regimes of the nanowire:

$$\chi = (\bar{r}_s - \bar{r}_c). \tag{12}$$

Substitution of this expression in Eq. (10) gives a simple expression for $\beta_{\rm nw}$:

$$\beta_{\rm nw} = 3\frac{d\ln\bar{r}_c}{dT} + \frac{d\ln\left[1+\frac{N_s}{N_c}\left(1+\frac{\chi}{\bar{r}_c}\right)^3\right]}{dT}. \tag{13}$$

Calculation of the expansion coefficients of different parts of a nanowire thus requires the knowledge of temperature-dependent average bond lengths in the respective regimes. Nevertheless, if the above mentioned formulas are applied to MD data, a scaling is needed to account for the discrepancy between the MD simulation temperature and the actual temperature of the domain. Because the actual temperature must involve quantum mechanical effects that are particularly important at low temperatures [55]. The MD-temperature is however well-correlated with the actual temperature by the following [61–63]:

$$T_{\rm md} = \frac{1}{k_b}\int \hbar\omega D(\omega)\left(\frac{1}{2} + \frac{1}{\exp\frac{\hbar\omega}{k_bT}-1}\right)d\omega, \tag{14}$$

where $D(\omega)$ is the phononic density of states. This expression has been demonstrated to produce experimentally consistent thermal properties of solids [64–69]. In principle, the first derivative of this relation scales the MD-obtained β to a corrected β that accounts for the quantum mechanical effect. Thus, if a relation of the form $T_{\rm md} = f(T)$ is known from phonon calculations, an accurate expression for the expansion coefficient β can be written as

$$\beta = \frac{1}{V_T}\frac{\partial V}{\partial T}\bigg|_p = \frac{1}{V_T}\left(\frac{\partial V}{\partial T_{\rm md}}\frac{\partial T_{\rm md}}{\partial T}\right)\bigg|_p \tag{15}$$

$$= \beta_{\rm md}\frac{dT_{\rm md}}{dT}, \tag{16}$$

where $\beta_{\rm md} \in \{\beta_{\rm nw}, \beta_{\rm core}, \beta_{\rm surface}, \beta_{\rm bulk}\}$ is the expansion coefficient obtained from MD-simulations.

Simulation details

Our simulations are divided into two parts. In the first part, we perform the density functional theory (DFT) simulations on a bulk SiC supercell containing eight atoms to obtain an accurate interatomic potential in the Stillinger-Weber form [70] (which we denote as the SW potential). The goal of this task is to derive a first-principle accurate anharmonic response of SiC over a large interatomic distance using a classical potential. In the second part we use the SW potential to perform MD simulations and investigate VTEC of bulk SiC and [111]-3*C*-SiC nanowires.

The DFT calculations are carried out using the open source software SIESTA [71]. The core electrons are replaced by norm conserving pseudopotentials following a Troullier and Martins scheme [72]. The valence electrons are represented by an extended numerical atomic basis set of polarized double-zeta (DZP) type. For the exchange-correlation part of the electron energy, we use the generalized gradient approximation (GGA) with the PBE functional [73]. The pseudopotentials (PP) for Si and C were obtained from the SIESTA pseudopotential database. In generating the PPs the valence configuration used for Si is $3s^2$, $3p^2$, $3d^0$, and $4f^0$ with a cutoff distance of 1.75, 1.94, 2.09, and 2.09 bohrs for the pseudoatomic orbitals (PAOs), respectively. For C, the valence configuration used was $2s^2$, $2p^2$, $3d^0$, and $4f^0$ with a cutoff at 1.54 bohrs for all the PAOs. The calculations are performed with an energy threshold of 1.0×10^{-4} eV per supercell and a force tolerance of 0.01 eV/Å to ensure convergence of the results. The relaxation of atoms is carried out by using the conjugate gradient optimizer with a maximum displacement of 0.05 Å and the energy cutoff for the basis is 50 meV.

The periodic supercell containing eight atoms is subjected to hydrostatic deformation for 100 different values of interatomic distance and at each of these deformed states the energy per atom is calculated. The equilibrium structural parameters of the lattice (a_0, k_b, and E_c) is then extracted from the energy versus interatomic distance curve. These properties are then used in developing the parameters for the SW potential. At each deformation state only the atoms were allowed to relax, keeping the volume of the supercell fixed. The Brillouin zone (BZ) integration is performed with a Monkhorst-Pack (MP) k mesh of $10\times10\times10$ that resulted in 560 k points in the reciprocal space of the domain. From the energy versus lattice constant data the equilibrium lattice constant is found to be $a_0 = 4.385$ Å, which agrees with the experimental value of 4.36 Å [74] within 0.67%.

For the MD simulations, the SW-potential parameters are obtained using the procedure outlined elsewhere [75], here we provide brief details for completeness. In general, the SW potential models many-body interaction of a solid through a sum over two-body $V_2(r_{ij})$ and three-body $V_3(\theta_{ijk})$ interactions terminated by a cutoff distance r_c. The mathematical forms of V_2 and V_3 are

$$V_2(r_{ij}) = A\epsilon\left(B\frac{\sigma^4}{r_{ij}^4} - 1\right)\exp\left(\frac{\sigma}{r_{ij}-r_c}\right), \tag{17}$$

$$V_3(\theta_{ijk}) = \lambda\epsilon(\cos\theta_{ijk} - \cos\theta_0)^2\exp\left(\frac{2\gamma\sigma}{r_{ij}-r_c}\right). \tag{18}$$

Here, r_{ij} is the distance between atoms located at r_i and r_j; $\theta_{ijk} = \arccos\frac{\hat{r}_{ij}\cdot\hat{r}_{ik}}{|\hat{r}_{ij}||\hat{r}_{ik}|}$ is the angle between the bonds r_{ij} and r_{ik} formed at site i; and $A, B, \epsilon, \sigma, \lambda, \gamma$ are the SW parameters. The parameters A, B, σ, and λ are obtained from DFT-generated force-constant K_b, cohesive energy E_c, bond bending constant k_θ, and equilibrium bond length r_0. Among the remaining parameters of the SW potential, we take r_c as the second-neighbor distance and exploit the free parameters γ and ϵ to calibrate the potential up to the maximum force point in the force-strain curve. For modeling, the two-body and three-body interactions

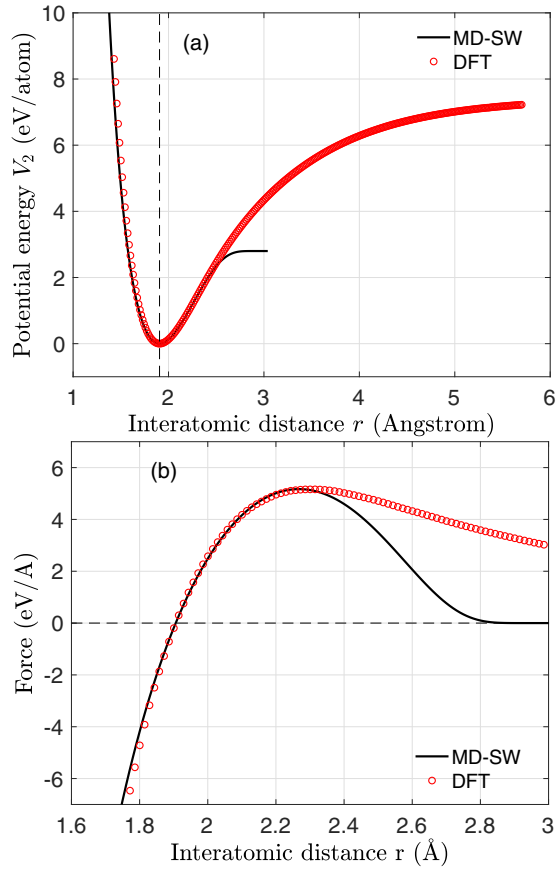

FIG. 1. (a) Comparison of the MD-SW potential function with DFT-GGA data points under hydrostatic deformation. The vertical dashed line indicates the equilibrium bond length of 1.90590 Å. (b) Comparison of the MD-SW forcing function with the corresponding DFT-GGA data points. The horizontal dashed line indicates the zero force line.

(denoted by C-Si-Si or Si-C-C in LAMMPS notation), we determine the following SW parameters following the above mentioned procedure: $\epsilon = 1.9$, $\sigma = 2.4050$, $a = 1.26819$, $\lambda = 19.0, \gamma = 0.69000$, $\cos\theta = -0.33333$, $A = 11.30864$, and $B = 0.18411$. It should be noted that in crystalline bulk SiC or nanowire SiC there is no Si-Si or C-C bonds within the cutoff distance r_c, which is taken less than the second-neighbor distance. So, for modeling the behavior of the lattice under consideration, the parameters describing Si-Si, C-C two-body interactions and C-C-Si, C-Si-C, Si-C-Si, Si-Si-C three-body interactions are not needed. However, to model an amorphous phase or defect structures wherein C-C or Si-Si appear within the cutoff distance, a set of other SW parameters are needed to account for the relevant two-body and three-body interactions.

The resulting energy-distance and force-distance curves are compared with DFT in Fig. 1, which indicates reasonable agreement between the DFT-GGA and MD-SW results over the entire regime of interatomic distances that are relevant for studying thermal expansion of the material. The MD-SW reproduces the DFT-GGA generated forcing function up to the maximum force and to match with the cohesive energy of the solid an energy correction is needed [75], which does not affect any energetics or forcing behavior of the solid up to the bond length at which the bond length is a maximum. Thus this energy correction or the difference between the MD potential energy and DFT-GGA potential energy at $d \to \infty$ yields a constant potential energy correction: $\Delta E_{\text{correction}}$ which is calculated as 3.40 eV/atom. This energy correction has no implication on the forcing behavior as its derivative produces zero contribution to force. Also, for the highest temperature considered in this work, the anharmonicity is contained within a very small bond length window surrounding the equilibrium point.

The MD simulations are performed using the open source code large-scale atomic/molecular massively parallel simulator (LAMMPS) [76]. In these simulations, we first relax the system statically to get rid of any residual stress by applying the conjugate gradient minimizer. Then assigning a random velocity distribution to the atoms representing a temperature of 1 K, we raise the temperature of the system to a target temperature over a period of 5 ns by applying the Noose-Hoover thermostat. During this equilibration process zero pressure is maintained by applying the Anderson barostat using the isobaric and isothermal ensemble. The simulations are performed with a time step of 1.0 fs, and the parameters for thermal and pressure damping were selected as 1 and 10 ps, respectively. Periodic boundary condition is employed along all directions in modeling thermal expansion for the bulk SiC configuration. In modeling thermal expansion of the nanowires, periodic condition is applied only along the longitudinal or [111] direction of the nanowire, and an empty space is included in the lateral directions sufficiently large to avoid interactions among the periodic images of the NWs.

III. RESULTS AND DISCUSSIONS

First we investigate β_{bulk} and establish the bond length based framework to obtain reliable prediction of β from atomistic data. We then apply the framework to determine the βs for the nanowires and evaluate the relative contributions of the surface versus core regimes on overall thermal expansion coefficient of the nanowire, or β_{nw}.

A. VTEC of bulk 3C-SiC

In determining VTEC for bulk SiC using Eq. (5), we calculate $\bar{r}$ from a periodic supercell containing 24 800 atoms at 17 different temperatures ranging from 1 to 2100 K with an interval of 150 K. The supercell's orthogonal sides are bounded by planes with normal directions aligned along the [111], [$\bar{1}$10], and [11$\bar{2}$] directions. The ensemble average bond length is calculated from the ensemble averaged mean bond length: $\bar{r} = \sum \bar{r}_i/N$, where $\bar{r}_i$ is the average length of the bonds connected with atom i, where $i = 1, 2, \ldots, N$ with N being the total number of atoms. To evaluate the accuracy of this mean-based estimation, we analyze the role of skewness on the central tendency of $\bar{r}$ by computing the radial distribution function at a few temperatures. As depicted in Fig. 2, at $T = 1$ K, the distribution of the bond length is a normal distribution with zero variance. The mean and median based estimations produce a unique value of $\bar{r}$. However, at higher temperatures, say at $T = 900$ K, they differ due to

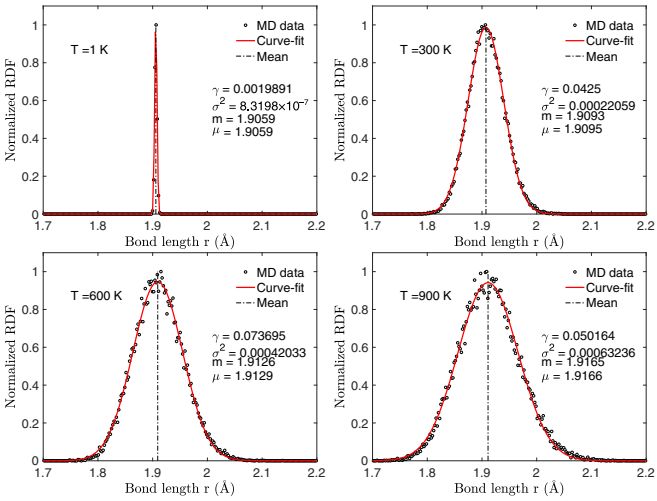

FIG. 2. Normalized radial distribution function (RDF) $g(r)/g_{\max}(r)$ of the bond lengths in bulk SiC at 1, 300, 600, and 900 K. The statistical properties of the MD data, mean μ, variance σ^2, median m, and skewness γ are given in the plots.

the right-skewed feature of the distribution—but the variance is substantially small as long as the number of atoms in the domain is sufficiently large to avoid the effect of thermal fluctuation in bond lengths. The mean-based calculations is thus found to be a reliable measure of $\bar{r}$.

Using the ensemble averaged bond length $\bar{r}$, we calculate temperature-dependent linear thermal expansion coefficient $\alpha(T)$ from Eq. (5), using the second-order accurate central difference numerical scheme for discretizing the derivative. Results obtained on $\alpha(T)$ from our MD calculations are compared with those of available experimental [13] and analytical results [57]. As seen from Fig. 3, they exhibit reasonable agreement over the entire temperature regime, except at temperatures lower than 600 K. In that temperature regime, our MD-SW results show closer agreement with the analytical results. Also, the higher temperature behavior of α is consistent across MD-SW data, experimental measurements, and the analytical results. Since our MD-SW potential is, by construction, a nearest-neighbor model that accounts for interactions within the second-neighbor distance only, its close agreement with the experimental and analytical results highlights the thermal expansion behavior to be dominated by interactions bounded by the second-nearest-neighbor distance.

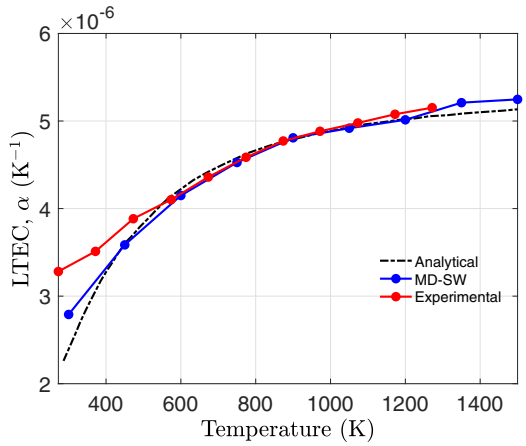

FIG. 3. Temperature-dependent linear thermal expansion coefficient (LTEC) or α of bulk 3C-SiC obtained from MD-SW simulations, experimental and analytical results.

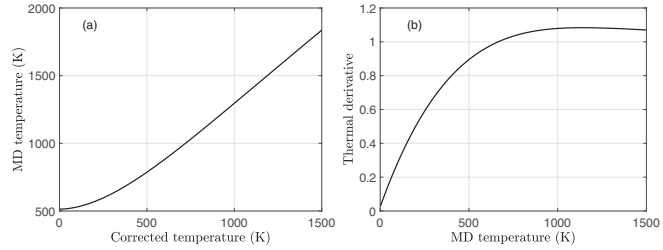

FIG. 4. (a) MD temperature vs actual temperature and (b) thermal derivative $dT_{\rm md}/dT$ at different temperatures.

In correcting the MD temperature and to account for the quantum mechanical effects on thermal expansion, the scaling factor $dT_{\rm md}/dT$, appearing in Eq. (16), is obtained from the relation between the corrected MD temperature and the actual temperature of the system, $T_{\rm md} = 513.45 - 0.18635T + 0.0014644T^2 - 9.8586 \times 10^{-7}T^3 + 3.4008 \times 10^{-10}T^4 - 4.6948 \times 10^{-14}T^5$, proposed for bulk SiC in Ref. [58]. See Fig. 4. The quantity $dT_{\rm md}/dT$ obtained from this available literature data resulted in smaller values of α at each T, when compared with the analytical results. Addition of a constant value however produced reliable estimates of α, as shown in Fig. 3. The expression for $T_{\rm md} = 513.45 + 0.025T + 0.5 \times 0.0029288T^2 - (1/3) \times 29.5758 \times 10^{-7}T^3 + 0.25 \times 13.6032 \times^{-10} T^4 - 0.20 \times 23.4740 \times 10^{-14}T^5$ and thermal derivative as: $dT_{\rm md}/dT = 0.025 + 0.0029288T - 29.5758 \times 10^{-7}T^2 + \times 13.6032 \times^{-10} T^3 - 23.4740 \times 10^{-14}T^4$. The resulting curves are shown in Fig. 4, which indicates $T_{\rm md} > T$ below 700 K and $T_{\rm md} < T$ above 700 K.

Based on the reasonably accurate prediction of $\beta_{\rm bulk}$ by the MD-SW potential as well as the close agreement between the DFT-GGA and MD-SW potential and force functions (that form the basis for the anharmonic response of the lattice), we consider the MD-SW potential and the bond length based atomistic framework as a reliable set of tools to investigate the expansion behavior of SiC nanowires. In calculating β for the nanowires, we use the same scaling $dT_{\rm md}/dT$ obtained here for bulk SiC, assuming the scaling to be a material-dependent quantity and independent of atomic configuration.

B. VTEC of nanowire 3*C*-SiC

1. Defining the core and surface regimes

For the nanowire calculations, we create their atomistic configurations from an orthorombic unit cell of SiC comprising twelve atoms bounded by the following lattice vectors:

$$a_1 = 3(r_0 + (\sin\phi - \sqrt{2}\cos\phi)/4),$$
$$a_2 = 6(-\sin\phi\sin\theta + \cos\phi + \sin\phi\cos\theta)a/4,$$

and,

$$a_3 = (\sin\theta + \cos\theta)a/2,$$

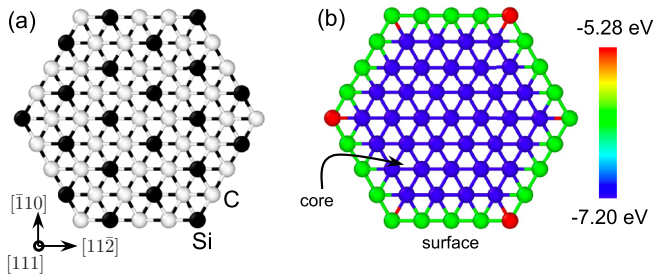

FIG. 5. (a) Cross sectional view of an [111]-SiC nanowire of 1.3 nm diameter with the [111] direction along its longitudinal axis and the lateral directions are [$\bar{1}$10] and [11$\bar{2}$]. Atoms are identified as Si and C. (b) Potential energy map across the nanowire cross-section showing the core and surface regions.

where $\theta = \pi/4$ and $\phi = \arctan\frac{1}{\sqrt{2}}$. The atomic coordinates are $\vec{r}_1 = (0, 0, r_0 + 2\delta_1)$, $\vec{r}_2 = (\delta_2, a_3/2, 0, 0)$, $\vec{r}_3 = (2\delta_2, 0, \delta_1)$, $\vec{r}_4 = (3\delta_2, a_3/2, 2\delta_1)$, $\vec{r}_5 = (4\delta_2, 0, 0)$, $\vec{r}_6 = (5\delta_2, a_3/2, \delta_1)$, $\vec{r}_7 = (0, 0, r_0 + 2\delta_1, 2r_0 + 2\delta_1)$, $\vec{r}_8 = (\delta_2, a_3/2, 0, 2r_0 + 3\delta_1)$, $\vec{r}_9 = (2\delta_2, 0, r_0 + \delta_1)$, $\vec{r}_{10} = (3\delta_2, a_3/2, 2r_0 + 2\delta_1)$, $\vec{r}_{11} = (4\delta_2, 0, 2r_0 + 3\delta_1)$, and $\vec{r}_{12} = (5\delta_2, a_3/2, r_0 + \delta_1)$. Here, $\delta_1 = s_\phi a/4 - c_\phi a/(2\sqrt{2})$, $\delta_2 = (-s_\phi s_\theta + c_\phi + s_\phi c_\theta)a/4$ and $\delta_3 = (s_\theta + c_\theta)a/4$ are the interplanar spacing along the [111], [11$\bar{2}$], and [$\bar{1}$10] directions, respectively; $r_0 = 1.905$ Å is the equilibrium bond length; and $a = 4.4015$ Å is the equilibrium lattice constant of our SiC-SW potential which agrees with the corresponding lattice parameter of 4.385 Å obtained from our DFT-GGA calculation and with the experimental value of 4.36 Å [77,78] within 1%. Figure 5 illustrates the cross-section of an example [111]-SiC nanowire and the potential energy map in the initial condition.

Here we used the potential energy density variation across the nanowire's cross-section to define the core and surface regimes. It is clear that the bulk atoms with four nearest neighbors are the lowest potential energy density atoms, and the atoms at the six corners containing two nearest neighbors are the highest potential energy density atoms, and the atoms on the edges or sides containing three nearest neighbors are the atoms with the intermediate potential energy density. We define the atoms with the nearest neighbors less than 4 as the surface atoms, and the atoms with four nearest neighbors as the core atoms. Furthermore, as evident from Fig. 6, the average bond lengths in the core and surface regimes are reasonably approximated to be uniform in the respective regimes.

We calculated the average bond length at different radial distance from the nanowire center by averaging over the bond lengths at the atoms in the atomic-columns normal to the {111} plane. At 300 K, the lateral fluctuations are not visible for the atomic representation of the configuration shown in the figure, while at 1500 K, an indication of the atomic fluctuations is evident. Each data point shown by filled circles represents the average location of the atoms in the (x, y) plane, and the error bar shows the deviation of the average value at different time steps during the dynamic equilibrium of the system at a spatial location from the center. The plots suggest that the higher the temperature is, the higher is the difference in values of the average bond lengths between the

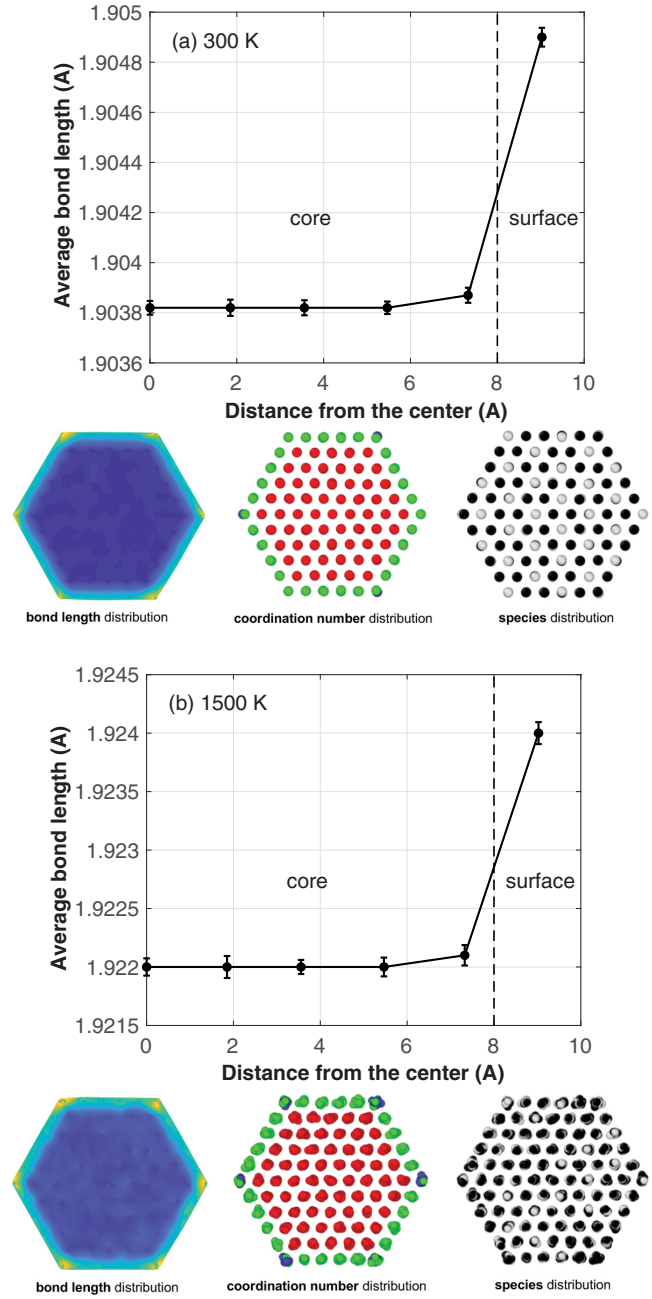

FIG. 6. Bond length variation across the nanowire cross section, relative to the center in $d = 17.73$ Å nanowire at (a) 300 and (b) 1500 K. The maps of bond length, nearest-neighbor coordination number, and species distributions are shown at the bottom of each plot. The coordination number varies from 2 (blue spheres) to 4 (red spheres) and the species are Si (black spheres) and C (ash spheres).The vertical dashed line denotes the transition between the core regime and the surface regime.

surface versus core regimes. Furthermore, the distinction of the two surface and core regimes is closely related with the potential energy density across the nanowire's cross-section. We thus consider the potential energy density as a basis for decomposing the nanowire's cross-section into the bulk and surface regions. It should be emphasized that the potential energy density correlates directly with the stiffening and

softening state of the bond, and thereby can directly affect the thermal expansion coefficient of the nanowire. Because expansion coefficient by definition is related to the change in length (not the actual length itself). Thus missing neighbors (reflected in the potential energy density variation) has the dominant effect on thermal expansion.

Since the nanowire is periodic along its axial direction and finite along the lateral directions, we explore the stress state of the atoms in the nanowire to determine if the thermal oscillation is anisotropic. Calculating the Virial atomic stress components at each atomic site and determining the ensemble averaged normal atomic stresses in the nanowire, we find them to match within 0.1%, at each of the temperatures considered between 1 to 1500 K. It is thus reasonable to conclude: $\sigma_{xx} = \sigma_{yy} = \sigma_{zz}$ and the bonds oscillate isotropically, at least locally, in the nanowire.

2. *Diameter-dependent thermal expansion*

Taking ten unit cells along the [111] direction, we consider twenty diameters ranging from 0.98 to 6.53 nm. Each of the nanowires is then equilibrated at 17 different temperatures separately. Then employing Eqs. (8) to (10) the volumetric thermal expansion coefficients $\beta_{\rm nw}$, β_c, and β_s are obtained for all the nanowires. The results presented in Fig. 7 suggest a number of important features of thermal expansion in SiC NWs: (i) $\beta_{\rm nw}$ is diameter independent at temperatures less than 100 K; (ii) at higher temperatures $T > 1000$ K, $\beta_{\rm nw}$ is strongly dependent on diameter: the smaller the diameter is, the higher is the value of $\beta_{\rm nw}$; (iii) similar to bulk SiC, $\beta_{\rm nw}$ increases rapidly at lower temperatures followed by a slower increase at higher temperatures; (iv) $\beta_{\rm surface} > \beta_{\rm core}$ for nanowires with $d > 1$ nm; (v) beyond $d = 1.3$ nm $\beta_{\rm surface}$ has negligible dependence on diameter; and (vi) for $d > 1$ nm there is a sizable difference between the expansion coefficients of bulk SiC and NW SiC at higher temperatures, so that $\beta_{\rm nw} - \beta_{\rm bulk} \neq 0$. The last observation suggests a sustaining effect of the surface in the nanowire.

To construct a quantitative picture of the diameter-dependent expansion behavior, we represent the diameter-dependent variations of β at $T = 300$ and 1500 K in Fig. 8. This figure provides some additional features of thermal expansion in SiC NWs: (a) nanowires of $d < 1$ nm, exhibit substantially higher expansion compared to the rest nanowires; (b) thermal expansion of thinner NWs is highly sensitive to diameter change compared to that of thicker NWs; and (c) for nanowires with $d > 1$ nm $\beta_{\rm nw}$ is dominated by $\beta_{\rm core}$; and (d) for most of the nanowires considered: $\beta_{\rm s} > \beta_{\rm nw} > \beta_{\rm c} > \beta_{\rm bulk}$. At 1500 K, $\beta_{\rm surface}$ of $d = 0.98$ nm NW is 1.67 times that of $d = 6.53$ nm, while $\beta_{\rm core}$ of $d = 0.98$ nm NW is 1.45 times that of $d = 6.53$ nm.

Although the MD results show that $\beta_{\rm nw} - \beta_{\rm bulk} > 0$ for the largest diameter considered—there is a trend that the values of β continue to diminish with increasing diameter, suggesting the possibility of $\beta_{\rm nw} \to \beta_{\rm bulk}$ with $d \to \infty$. Thus, at constant temperature, diameter-dependent expansion coefficients of the nanowire, core, and surface are fitted to the following function:

$$\beta(d) = \beta_0\left(1 + \frac{p}{d^n}\right), \tag{19}$$

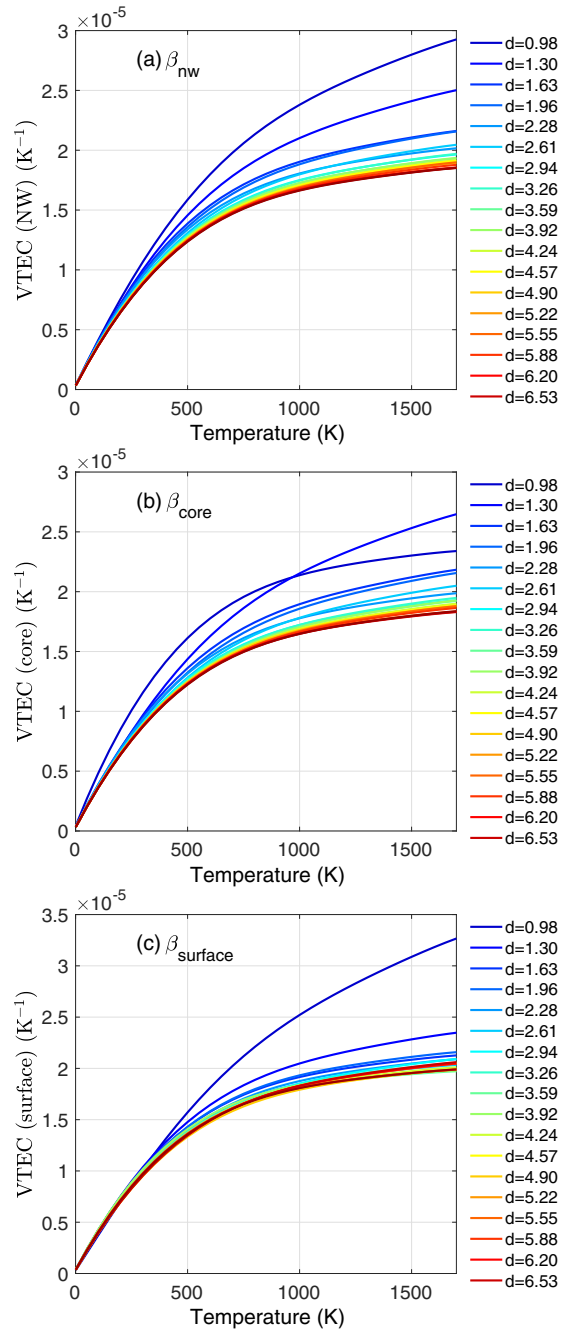

FIG. 7. Diameter-dependent volumetric thermal expansion coefficient in (a) nanowire, (b) core, and (c) surface in nanowires of diameter ranging from 0.98 to 6.53 nm at different temperatures spanning 1 to 1500 K.

where β_0 denotes the volumetric expansion coefficient of the nanowire with $d \to \infty$, and p and n are the fitting constants that fit the MD generated β versus diameter data. Both of the fitting parameters and β_0 depend on the system temperature T. In Table I, we provide their values at 300 and 1500 K. Results indicate that $\beta_0 \approx \beta_{\rm bulk}$ for the expansion coefficients of the nanowire and the core. Here the values of $\beta_{\rm bulk}$ is obtained from the linear thermal expansion coefficient (presented in Fig. 3) using the relation that the volumetric expansion coefficient is three times the linear thermal expansion coefficient.

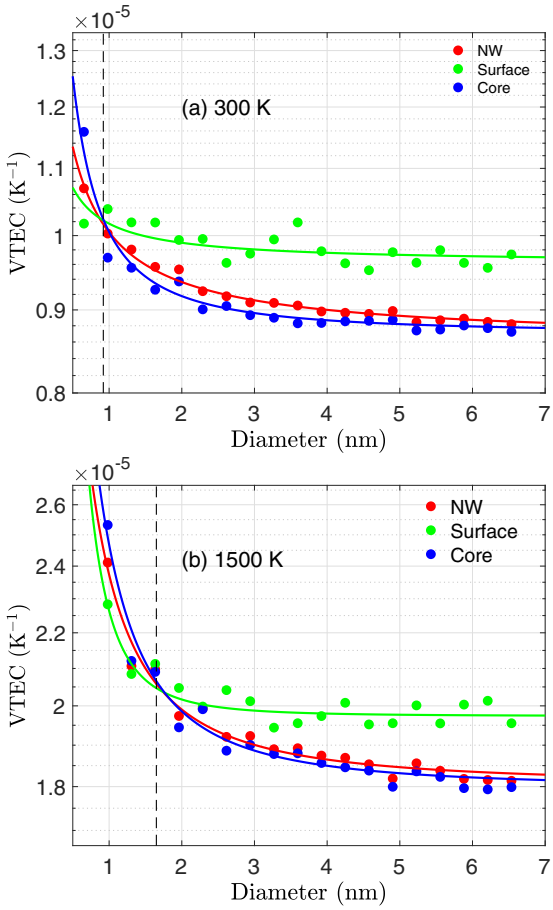

FIG. 8. Diameter-dependent β at (a) 300 and (b) 1500 K. The dashed vertical line in each plot indicates the value of d at which $\beta_{\text{core}} = \beta_{\text{surface}}$.

The physical basis for the inverse dependence comes from a vanishing effect of the surface atoms with increasing diameter. Similar functional dependence is reported for size-dependent thermodynamic properties of metallic nanoparticles as well [8]. Yet the diameter dependence of the core and surface vary differently with respect to a change in diameter. At $T = 300$ K, the observed behavior is well characterized by the surface-area-to-volume ratio which varies as $2/d$; whereas, at $T = 1500$ K, the diameter-dependent reduction in expansion coefficients is sharper than $2/d$. In either of the temperature regimes, β_{nw} is largely dominated by β_{core}. Thus a measurement of the expansion coefficient from macroscopic dimension of the nanowire would underestimate the expansion coefficient of the surface and the expansion coefficient of the core is accurately captured by the nanowire's expansion coefficient. Moreover it is evident that the NWs with diameters less than 1 nm behave differently from the nanowires with larger diameters. In the next section, we look for the atomistic basis for the difference in VTEC between surface and core and explore the origin of the inverse diameter dependence of β_{nw}.

TABLE I. Fitting parameters describing the diameter-dependent expansion coefficient in SiC nanowire. The goodness-of-fit is computed using the R^2 measure and given below. The units of a_0 and a_1 are K^{-1} and $\text{nm}^n\,\text{K}^{-1}$, respectively; and n is dimensionless.

Parameter					Fit accuracy
T	β	β_0	p	n	R^2
300	NW	8.593×10^{-5}	0.17	0.9177	0.9886
300	Core	8.700×10^{-6}	0.15	1.5	0.9566
300	Surface	9.613×10^{-6}	0.58	0.9658	0.5298
1500	NW	1.803×10^{-5}	0.31	1.607	0.9711
1500	Core	1.79×10^{-5}	0.37	1.826	0.9667
1500	Surface	1.973×10^{-5}	0.15	2.75	0.8654

3. *Atomistic basis*

To uncover the theoretical basis behind the observation that $\beta_s > \beta_c$ and $\beta_{\text{nw}} > \beta_{\text{bulk}}$ at temperatures higher than the room temperature, we compare Eqs. (13) and (5). For sufficiently larger diameter nanowires, the number of surface atoms is substantially less than the number of core atoms, so that it is reasonable to assume $N_s/N_c \to 0$, which yields the following difference between the coefficients of the bulk and nanowire:

$$\beta_{\text{nw}} - \beta_{\text{bulk}} = 3\left(\frac{d\ln\bar{r}_c}{dT} - \frac{d\ln\bar{r}_b}{dT}\right) \tag{20}$$

$$= 3\frac{d}{dT}\ln\left(1 + \frac{\chi_c}{\bar{r}_b}\right), \tag{21}$$

where $\chi_c = \bar{r}_c - \bar{r}_b$ is the differential anharmonicity of the core atoms in the nanowire relative to the bulk. As evident from this relation, $\beta_{\text{nw}} \to \beta_{\text{bulk}}$ only if $\chi_c \to 0$. The observation from our MD results that $\beta_{\text{nw}} > \beta_{\text{bulk}}$ indicates a sustaining existence of differential anharmonicity χ_c in the nanowire, even for larger diameter. Although it can be conjectured that with $d \to \infty$ $\beta_{\text{nw}} \to \beta_{\text{bulk}}$, for all the nanowires whose dimensions are by definition in the nanoscale, we predict $\beta_{\text{nw}} - \beta_{\text{bulk}} \neq 0$. This analysis gives a qualitative phenomenological understanding of the role of nanowire size on its thermal expansion behavior. It is clear that for a sufficiently large diameter nanowire, there is still nonuniformity in anharmonicity but it is of much lesser intensity due to less macroscopic thermal fluctuation of the system. The variation of β with diameter of NW shows the difference of average bond length of surface and core region to decrease in larger NWs. The dominance of surface atoms in material properties is minimized with the increase in NW diameter. To develop a quantitative measure of the anharmonic effects, we fit the radial distribution function (RDF), constructed from the atomic coordinates, with a normalized Gaussian function of the following form:

$$g(r) = \frac{4N}{w\sqrt{2\pi}}\exp - \frac{2(r-\bar{a})^2}{w^2}. \tag{22}$$

The difference between two RDFs, denoted here as the relative distribution or $\Delta g(r) = g(r) - g_{\text{ref}}(r)$ is then calculated to compare the harmonic and anharmonic parts of the distribution. Calculating $g(r)$ at 300 and 1500 K relative to 100 K for bulk SiC and the nanowires, we find that the bond length distribution to exhibit a larger deviation in nanowires compared to the bulk at higher temperatures, as depicted in Fig. 9. As expected the relative distribution confirms $\int_{r_0-\Delta r}^{r_0+\Delta r} \Delta g(r)dr =$

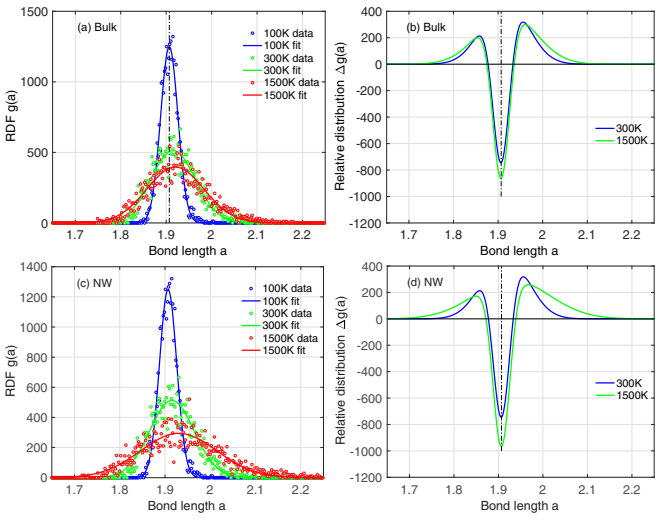

FIG. 9. Radial distribution function $g(r)$ at 100, 300, 1500 K in (a) bulk and (c) NW. The change in radial distribution function at 300 and 1500 K relative to that at 100 K is shown in (b) for the bulk and (d) for the NW. The diameter of the chosen NW is 1.56-nm nanowire.

0, where Δr is the maximum deviation of the bond length relative to the equilibrium bond length. The positive moment of the expansion side of the distribution is higher in NW compared to the bulk. Secondly, the deviation of the largest bond is much higher in nanowires compared to the bulk suggesting the presence of stronger heterogeneity in bond lengths in nanowires.

To determine if the nanowires (particularly the thinner ones) have melted at higher temperatures, we investigate RDFs for five nanowires of the smallest diameters at two different temperatures 300 and 1500 K. As shown in Fig. 10, there is apparent that the nanowires retain their solid phase even at 1500 K. However as expected, at higher temperature, the bond lengths are distributed over a wider range in all the nanowires.

Next to elucidate the individual contributions of the core and surface atoms in the expansion process, we decompose the contributions of the surface and bulk at different temperatures. From Eq. (8) and (9), the difference in expansion coefficients between the core and surface atoms in a given nanowire of diameter d is

$$\beta_s - \beta_c = 3\frac{d}{dT}\ln\left(\frac{\bar{r}_s}{\bar{r}_c}\right) \tag{23}$$

$$\Rightarrow \Delta\beta = 3\frac{d}{dT}\ln\left(1+\frac{\chi_s}{\bar{r}_c}\right), \tag{24}$$

where $\Delta\beta$ is the difference in thermal expansion coefficient between the surface and the core. This equation indicates that core and surface atoms would behave the same way if there's no differential anharmonicity present between their motion in a nanowire. From the MD results, it is seen that $\beta_s \approx \beta_c$ at lower temperatures—but with increasing T, $\beta_s - \beta_c$ increases for any choice of d. This suggests that $\chi_s \neq 0$ and the differential anharmonicity χ is temperature-dependent. The higher the temperature is, the higher is the differential anharmonicity in the nanowire. As the ratio of the surface versus core atoms

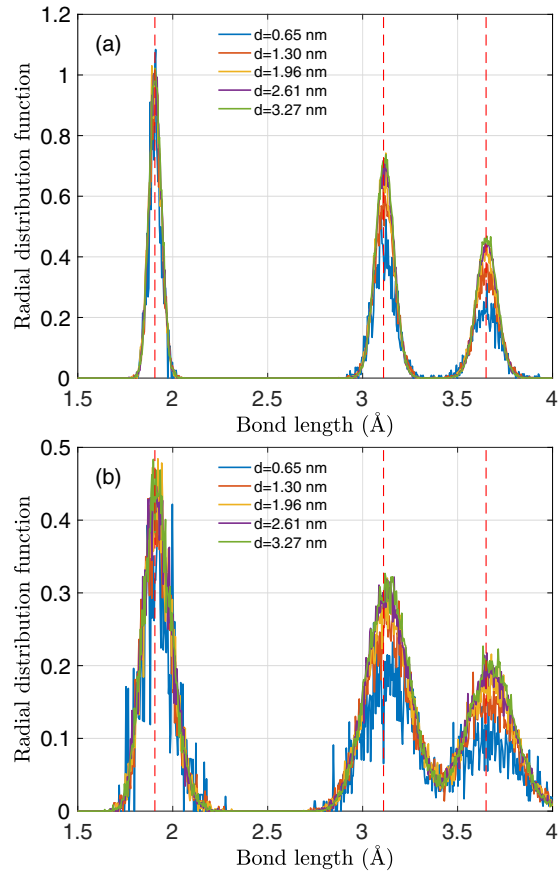

FIG. 10. Radial distribution function for five different nanowires at (a) 300 and (b) 1500 K. The dashed vertical lines represent the first-nearest-neighbor equilibrium distance of $r = 1.096$ Å, the second-nearest-neighbor of $r = 3.11$ Å, and the third-nearest-neighbor of $r = 3.65$ Å, respectively, at 1 K.

N_s/N_c remains constant in a nanowire (irrespective of the temperature), it has no effect on the distinct thermal expansion behavior of the core and surface. The differential anharmonicity is, however, depends on diameter, as evident from Fig. 11. In nanowires with $d < 1$, χ_s is negative—and for $d > 1$ nm, χ_s is positive. Results also suggest that the anharmonicity of the surface atoms saturates with $d \to \infty$, whereas the anharmonicity of the core atoms continues to decrease as a function of diameter. It can therefore be concluded that the diameter-dependent thermal expansion coefficients of the core and surface atoms, shown in Fig. 8, have a direct correlation with the differential anharmonicity presented in Fig. 11.

The observation of diameter-dependent differential anharmonicity can be explained from the stiffness and mass variation in the nanowires. From a simple spring-mass analysis, it is expected that both mass and bond stiffness have a direct influence on the displacement or anharmonic response of the mass. Since the volume or mass ratio of the surface versus core atoms explicitly affect thermal expansion [as seen in Eq. (13)], we investigate the volumes of core and surface atoms denoted as V_{surface} and V_{core}, respectively, to examine their inertial effects. As illustrated in Fig. 12, V_{surface} and V_{core} show a transition diameter of $d_c = 1$ nm, whereat these quantities are equal. Below d_c the volume of the nanowire is dominated by the surface. Higher effective atomic mass at the surface

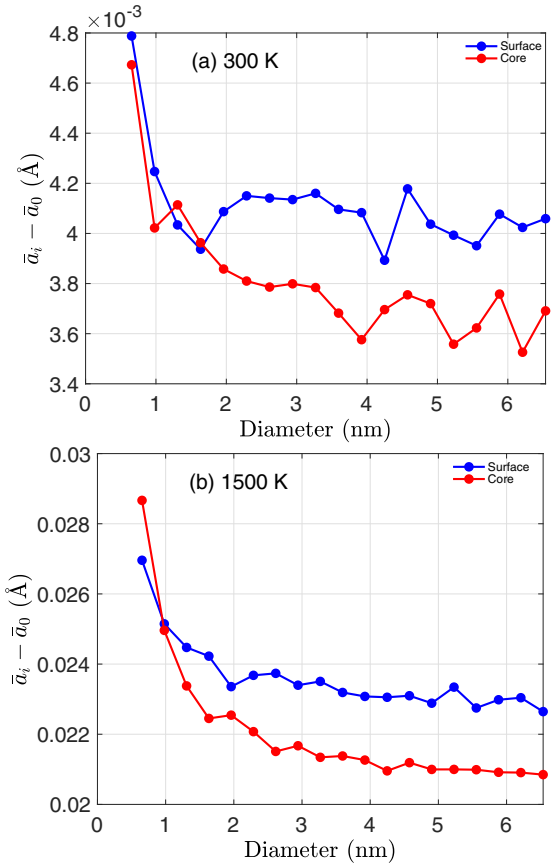

FIG. 11. Diameter-dependent anharmonicity at the core and surface at (a) 300 and (b) 1500 K.

can be deemed responsible for causing an inertial instability in nanowire's vibrational behavior. Also, the appearance of d_c can be assumed to be temperature independent, so that at any temperature there exists a diameter that demarcates the relative dominance of the inertial effects of the surface versus core. Thus the distinct behavior of thermal expansion

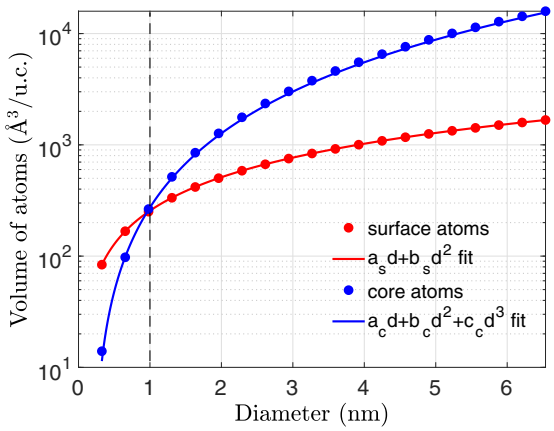

FIG. 12. Volume of surface atoms vs volume of core atoms as a function of diameter at 300 K. The vertical line shows the transition diameter that identifies the dominance of the atoms: the left side is dominated by the surface atoms and the right side by the core atoms. The dashed vertical line indicates the transition diameter d_c.

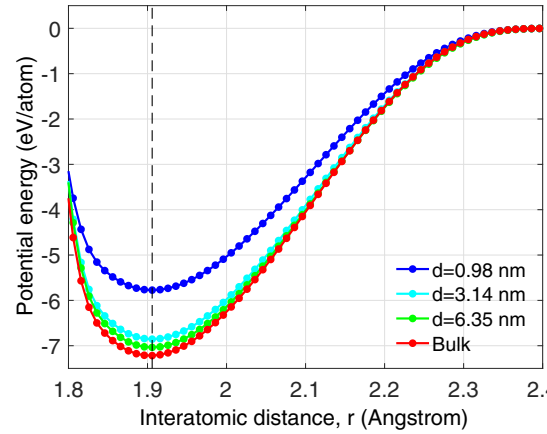

FIG. 13. Interatomic potential energy per atom for bulk SiC and for a set of SiC NWs with different diameters. The energy curves are obtained from deforming the nanowires hydrostatically (which gives similar atomic configuration under the influence of temperature change) and determining the energy per atom at each deformed state of the nanowire. The dashed vertical line indicates the equilibrium bond length r_0.

in regimes $d < 1$ nm and $d > 1$ nm can be deemed to arise from the volume or mass ratio between the surface and core.

Furthermore, as shown before, the nanowires of different diameters at equilibrium are at different mechanical state due to the presence of the surface atoms. If the temperature of the nanowires is increased from 0 to, say, 1000 K (whereat the average thermal energy per atom for any of the nanowires in equilibrium is $3k_bT/2 = 1.5 \times 8.6173303 \times 10^{-5} \times 1000 = 0.13$ eV, where k_b is the Boltzmann constant), the nanowires of different diameter respond to the energetic modulation differently due to their differential energetic/mechanical state at 0 K. The anharmonicity is thus different in nanowires versus bulk.

In addition to the inertial effects, anharmonicity in thermal motion is affected by the stiffness of the bonds that are prescribed by the curvature of the potential energy density variation in the nanowire as a function of the diameter. The higher the diameter of the nanowire is, the stiffer is the nanowire is and, thereby, the higher is the degree of anharmonicity (or the deviation of the mean position of the vibrating atoms relative to the equilibrium state), as exhibited in Figs. 13 and 14.

It is evident that presence of surface substantially affects the effective stiffness of the nanowire. For nanowires of $d < 1$ nm, the bonds are much softer than the bulk. With increasing diameter, the effective stiffness of the nanowires approaches the bulk value, thus makes the anharmonicity of thicker nanowires closer to the bulk. The difference between the potential energy density $\Delta E = E_{\text{nw}} - E_{\text{bulk}}$ accounts for the surface-energy per atom or $\Delta E/N$, where N is the total number of atoms in the nanowire. Effect of the surface atoms on ΔE can be estimated from $\Delta E_s = (E_{\text{nw}} - E_{\text{bulk}})/N_{\text{surface atoms}}$, which is much higher than the ensemble averaged ΔE. Since the potential energy per atom is higher at the surface, the atoms at the surface dominate the vibrational energetics in smaller nanowires as ΔE is higher in smaller diameter nanowires. Compared to the bulk atoms which have four nearest neighbors (NNs), the surface atoms bonded with three

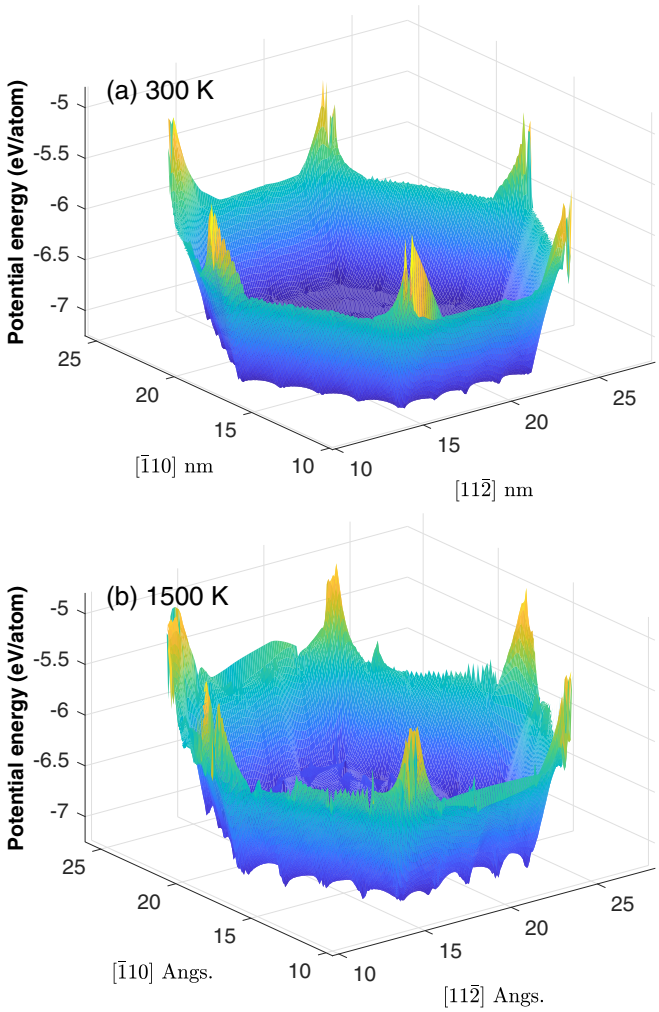

FIG. 14. Average potential energy density variation across the nanowire cross-section at (a) 300 and (b) 1500 K. The range of potential energy density at 300K is −5.26 to −7.35 eV/atom, while at 1500 K it is −4.83 to −7.31 eV/atom indicating increased energy density and higher variation at higher temperature.

NNs have at least 25% less potential energy, and the atoms with two NNs have at least 50% less potential energy. The bond-deficient surface atoms have more compliant effective bonds. For a given energy ΔE, the energetic drive to stretch out of equilibrium is much higher for the surface atoms than the bulk, for the reason that a compliant spring must stretch more than a stiff spring as a response to a given energetic perturbation. Therefore the surface atoms have higher expansion coefficients in thicker nanowires, whereas in thinner nanowires the behavior is governed by a combination of inertial effects and stiffness of the bond.

IV. CONCLUSION

In conclusion, this paper presents a bond-length based computational framework to unveil the distinctive thermal expansion coefficients of surface and core atoms in [111] 3*C*-SiC over a wide diameter range (covering 0.98-nm to 6.53-nm nanowires). Results show that in thicker nanowires the anharmonic response of the surface atoms is much more pronounced compared to that of the core atoms at higher temperatures. In thinner nanowires, the expansion of both the surface and core atoms are substantially higher than the bulk. The comparative analysis of the surface and core effects shows the core atoms to make the dominant contribution to the overall thermal expansion in the nanowires in thicker nanowires, whereas in thinner nanowires, the surface and core atoms play an equal role.

Additionally, temperature-dependent expansion behavior of SiC nanowires exhibits a continued increase of the expansion coefficient at the core and surface as well as in the nanowire, with a diminishing trend at higher temperatures. The expansion coefficient in bulk SiC dies down at temperatures beyond 1500 K, whereas there is a continued trend of increasing the expansion coefficients in the nanowire at the same temperature. This highlights enhanced sensitivity of thermal expansion in nanowires and suggests the possibility of tuning the effective thermomechanical behavior of nanocomposites by engineering the surface characteristics of nanowires. We attribute the enhanced sensitivity of thermal expansion to originate from a sustained differential anharmonicity in nanowires governed by variation in potential energy density across the nanowire cross-section. The atomistic methodology developed in this work is expected to address a key limitation of our current theoretical/computational tools in predicting thermal expansion in low-dimensional systems as well as in inhomogeneous systems (such as materials with surfaces or defects). Although the methodology outlined here is used for SiC bulk and nanowires of single surface type, we anticipate it to be applicable to nanowires of other materials and different surface orientations.

ACKNOWLEDGMENTS

Authors acknowledge the computing support provided by the FARBER computing facility at the University of Delaware. Authors thank the reviewers for offering insightful comments on the approach proposed in this work as well as on the discussions of the results and findings. Authors also thank Tianyi Weng for her help (through the undergraduate research program at UD) in generating some atomistic configurations at the initial stage of the work.

[1] S. Xiong, J. Ma, S. Volz, and T. Dumitric, Small **10**, 1756 (2014).

[2] T. Pavloudis, K. Termentzidis, P. Komninou, C. Latham, P. Briddon, and J. Kioseoglou, J. Appl. Phys. **119**, 074304 (2016).

[3] Y. Ni, S. Xiong, S. Volz, and T. Dumitrică, Phys. Rev. Lett. **113**, 124301 (2014).

[4] K. Termentzidis, M. Isaiev, A. Salnikova, I. Belabbas, D. Lacroix, and J. Kioseoglou, Phys. Chem. Chem. Phys. **20**, 5159 (2018).

[5] S. Xiong, B. Latour, Y. Ni, S. Volz, and Y. Chalopin, Phys. Rev. B **91**, 224307 (2015).
[6] S. Xiong, D. Selli, S. Neogi, and D. Donadio, Phys. Rev. B **95**, 180301 (2017).
[7] W. Huang, R. Sun, J. Tao, L. Menard, R. Nuzzo, and J. Zuo, Nat. Mater. **7**, 308 (2008).
[8] S. Xiong, W. Qi, Y. Cheng, B. Huang, M. Wang, and Y. Li, Phys. Chem. Chem. Phys. **13**, 10652 (2011).
[9] J. Diao, K. Gall, and M. L. Dunn, Nat. Mater. **2**, 656 (2003).
[10] J. Dugdale and D. MacDonald, Phys. Rev. **89**, 832 (1953).
[11] R. A. Schapery, J. Compos. Mater. **2**, 380 (1968).
[12] S. I. Novikova, Thermal expansion of solids (Izdatel'stvo Nauka, Moscow, 1974).
[13] G. A. Slack and S. Bartram, J. Appl. Phys. **46**, 89 (1975).
[14] R. Lakes, J. Mater. Sci. Lett. **15**, 475 (1996).
[15] R. Mittal, M. K. Gupta, and S. L. Chaplot, Prog. Mater. Sci. **92**, 360 (2018).
[16] R. Eloirdi, C. Giacobbe, P. A. Celdran, N. Magnani, G. H. Lander, J.-C. Griveau, E. Colineau, K. Miyake, and R. Caciuffo, Phys. Rev. B **95**, 094517 (2017).
[17] S. Li and Y. Chen, Phys. Rev. B **96**, 134104 (2017).
[18] D. T. Ho, S.-Y. Kwon, H. S. Park, and S. Y. Kim, Nano Lett. **17**, 5113 (2017).
[19] K. Takenaka, Y. Okamoto, T. Shinoda, N. Katayama, and Y. Sakai, Nat. Commun. **8**, 14102 (2017).
[20] H. Sun, L. Chen, S. Sun, and T.-Y. Zhang, Sci. China: Technol. Sci. **61**, 687 (2018).
[21] H. Zhu, Q. Li, C. Yang, Q. Zhang, Y. Ren, Q. Gao, N. Wang, K. Lin, J. Deng, J. Chen *et al.*, J. Am. Chem. Soc. **140**, 7403 (2018).
[22] X. Hu, P. Yasaei, J. Jokisaari, S. Öğüt, A. Salehi-Khojin, and R. F. Klie, Phys. Rev. Lett. **120**, 055902 (2018).
[23] D. Dvorak, A. Darbandi, K. L. Kavanagh, and S. P. Watkins, Nanotechnology **28**, 385302 (2017).
[24] G. Liu, B. R. Tuttle, and S. Dhar, Appl. Phys. Rev. **2**, 021307 (2015).
[25] P. J. Lamicq, Am. Ceram. Soc. Bull. **65**, 336 (1986).
[26] S. Wang, S. Dhar, S.-r. Wang, A. C. Ahyi, A. Franceschetti, J. R. Williams, L. C. Feldman, and S. T. Pantelides, Phys. Rev. Lett. **98**, 026101 (2007).
[27] J. Rozen, S. Dhar, M. Zvanut, J. Williams, and L. Feldman, J. Appl. Phys. **105**, 124506 (2009).
[28] J. B. Hannon, M. Copel, and R. M. Tromp, Phys. Rev. Lett. **107**, 166101 (2011).
[29] X. Shen and S. T. Pantelides, Appl. Phys. Lett. **98**, 053507 (2011).
[30] P. S. Branicio, J. Zhang, J. P. Rino, A. Nakano, R. K. Kalia, and P. Vashishta, Appl. Phys. Lett. **112**, 111909 (2018).
[31] S. Kwon, D.-K. Kim, M.-H. Cho, and K.-B. Chung, Thin Solid Films **645**, 102 (2018).
[32] J. Fan, X. Wu, and P. K. Chu, Prog. Mater. Sci. **51**, 983 (2006).
[33] A. Catellani, G. Galli, and F. Gygi, Phys. Rev. Lett. **77**, 5090 (1996).
[34] J. Kabel, Y. Yang, M. Balooch, C. Howard, T. Koyanagi, K. A. Terrani, Y. Katoh, and P. Hosemann, Composites Part B: Engineering **131**, 173 (2017).
[35] C. Real, J. M. Córdoba, and M. D. Alcalá, Ceram. Int. **44**, 14645 (2018).
[36] F. Gao, H. Xiao, X. Zu, M. Posselt, and W. J. Weber, Phys. Rev. Lett. **103**, 027405 (2009).
[37] L. Su, H. Wang, M. Niu, X. Fan, M. Ma, Z. Shi, and S.-W. Guo, ACS nano **12**, 3103 (2018).
[38] K. Yin, X. Su, Y. Yan, H. Tang, M. G. Kanatzidis, C. Uher, and X. Tang, Scr. Mater. **126**, 1 (2017).
[39] L. Yan, C. Hong, J. Liu, B. Du, S. Zhou, G. Zhao, P. Hu, and X. Zhang, ACS applied materials & interfaces **10**, 27955 (2018).
[40] F. Chen, G. Li, E. R. Zhao, J. Li, G. Hableel, J. E. Lemaster, Y. Bai, G. L. Sen, and J. V. Jokerst, Biomaterials **179**, 60 (2018).
[41] J. Zhao, Z. Li, X. Yuan, Z. Yang, M. Zhang, A. Meng, and Q. Li, Adv. Energy Mater. **8**, 1702787 (2018).
[42] S. Adhikari, N. K. Eswar, S. Sangita, D. Sarkar, and G. Madras, J. Photochem. Photobiol., A **357**, 118 (2018).
[43] Y. Cao, H. Dong, S. Pu, and X. Zhang, Nano Research **11**, 4074 (2018).
[44] B. Song, X. Zhang, P. He, G. Zhao, and G. Han, Int. J. Hydrogen Energy **42**, 20003 (2017).
[45] R. Wu, K. Zhou, C. Y. Yue, J. Wei, and Y. Pan, Prog. Mater. Sci. **72**, 1 (2015).
[46] J. Bai, Z. Yang, B. Dai, L. Yang, Q. Wang, J. Han, and J. Zhu, J. Mater. Sci. **53**, 13843 (2018).
[47] P. Hu, S. Dong, X. Zhang, K. Gui, G. Chen, and Z. Hu, Sci. Rep. **7**, 3011 (2017).
[48] P. W. Leu, A. Svizhenko, and K. Cho, Phys. Rev. B **77**, 235305 (2008).
[49] H. Liang, M. Upmanyu, and H. Huang, Phys. Rev. B **71**, 241403 (2005).
[50] N. Mameka, J. Markmann, and J. Weissmüller, Nat. Commun. **8**, 1976 (2017).
[51] F. Buda, R. Car, and M. Parrinello, Phys. Rev. B **41**, 1680 (1990).
[52] F. Elahi, L. Ma, and Z. M. Hossain, Phys. Rev. B **98**, 174111 (2018).
[53] P. Giannozzi, S. de Gironcoli, P. Pavone, and S. Baroni, Phys. Rev. B **43**, 7231 (1991).
[54] D. Strauch, Z. Phys. B **78**, 405 (1990).
[55] N. W. Ashcroft and N. D. Mermin, Solid State Physics, Vol. 403 (Holt, Rinehart and Winston, New York, 2005).
[56] K. Karch, P. Pavone, W. Windl, O. Schütt, and D. Strauch, Phys. Rev. B **50**, 17054 (1994).
[57] D. Talwar and J. C. Sherbondy, Appl. Phys. Lett. **67**, 3301 (1995).
[58] L. J. Porter, J. Li, and S. Yip, J. Nucl. Mater. **246**, 53 (1997).
[59] P. K. Schelling and P. Keblinski, Phys. Rev. B **68**, 035425 (2003).
[60] J. Che, T. Çağın, W. Deng, and W. A. Goddard III, J. Chem. Phys. **113**, 6888 (2000).
[61] C. Z. Wang, C. T. Chan, and K. M. Ho, Phys. Rev. B **42**, 11276 (1990).
[62] C. Goringe, D. Bowler, and E. Hernandez, Rep. Prog. Phys. **60**, 1447 (1997).
[63] A. P. Bartók, M. C. Payne, R. Kondor, and G. Csányi, Phys. Rev. Lett. **104**, 136403 (2010).
[64] J.-S. Wang, J. Wang, and J. Lü, Eur. Phys. J. B **62**, 381 (2008).
[65] E. Schwegler, J. C. Grossman, F. Gygi, and G. Galli, J. Chem. Phys. **121**, 5400 (2004).
[66] A. Togo and I. Tanaka, Scr. Mater. **108**, 1 (2015).
[67] T. Feng and X. Ruan, J. Nanomater. **2014**, 318757 (2014).
[68] R. Bianco, I. Errea, L. Paulatto, M. Calandra, and F. Mauri, Phys. Rev. B **96**, 014111 (2017).

[69] D.-B. Zhang, T. Sun, and R. M. Wentzcovitch, Phys. Rev. Lett. **112**, 058501 (2014).
[70] F. H. Stillinger and T. A. Weber, Phys. Rev. B **31**, 5262 (1985).
[71] J. M. Soler, E. Artacho, J. D. Gale, A. García, J. Junquera, P. Ordejón, and D. Sánchez-Portal, J. Phys.: Condens. Matter **14**, 2745 (2002).
[72] N. Troullier and J. L. Martins, Phys. Rev. B **43**, 1993 (1991).
[73] J. P. Perdew, K. Burke, and M. Ernzerhof, Phys. Rev. Lett. **77**, 3865 (1996).
[74] O. Auciello, J. Birrell, J. A. Carlisle, J. E. Gerbi, X. Xiao, B. Peng, and H. D. Espinosa, J. Phys.: Condens. Matter **16**, R539 (2004).
[75] M. Hossain, T. Hao, and B. Silverman, J. Phys.: Condens. Matter **30**, 055901 (2018).
[76] S. Plimpton, J. Comput. Phys. **117**, 1 (1995).
[77] G. L. Harris, *Properties of Silicon Carbide* (Institution of Engineering and Technology, 1995), p. 13.
[78] J. Oliveira, J. Morbec, and R. Miwa, J. Appl. Phys. **121**, 104302 (2017).